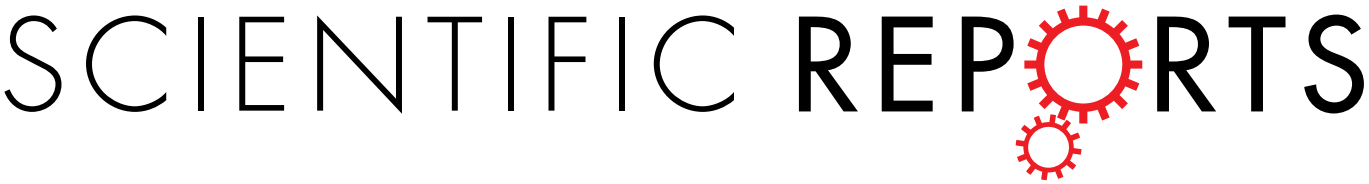

OPEN

Generation of a sub-diffraction hollow ring by shaping an azimuthally polarized wave

Received: 22 August 2016
Accepted: 01 November 2016
Published: 23 November 2016

Gang Chen[1], Zhi-xiang Wu[1], An-ping Yu[1], Zhi-hai Zhang[1], Zhong-quan Wen[1], Kun Zhang[1,2], Lu-ru Dai[2], Sen-lin Jiang[1], Yu-yan Li[1], Li Chen[1], Chang-tao Wang[3] & Xian-gang Luo[3]

The generation of a sub-diffraction optical hollow ring is of great interest in various applications, such as optical microscopy, optical tweezers, and nanolithography. Azimuthally polarized light is a good candidate for creating an optical hollow ring structure. Various of methods have been proposed theoretically for generation of sub-wavelength hollow ring by focusing azimuthally polarized light, but without experimental demonstrations, especially for sub-diffraction focusing. Super-oscillation is a promising approach for shaping sub-diffraction optical focusing. In this paper, a planar sub-diffraction diffractive lens is proposed, which has an ultra-long focal length of 600 λ and small numerical aperture of 0.64. A sub-diffraction hollow ring is experimentally created by shaping an azimuthally polarized wave. The full-width-at-half-maximum of the hollow ring is 0.61 λ, which is smaller than the lens diffraction limit 0.78 λ, and the observed largest sidelobe intensity is only 10% of the peak intensity.

In recent years, there has been a growing interest in generating and focusing cylindrically polarized waves due to their unique properties and possible application in light shaping[1]. The hollow rings have great potential in many optical applications, such as optical microscopy[2], optical tweezers[3], and nanolithography[4]. Reducing hollow ring size is of particular importance in further enhancing the optical resolution. Hollow focal spots can be generated by utilizing nanostructures[5] and the vortex phase plate[6]. An alternative way to generate a tight hollow ring is to focus an azimuthally polarized wave. Recently, special attention has been given to azimuthally polarized waves because of their unique properties in focusing and microscopy. Focusing of azimuthally polarized wave by high numerical aperture (NA) aplanatic lens has been extensively studied theoretically[6–14]. For a wavelength λ, a full width at half maximum (FWHM) of 0.24 λ of a ring size was theoretically predicted for an objective lens with a numerical aperture (NA) value of 1.4. However, its central ring peak was surrounded by a huge sidelobe ring, which was about 44 times larger than the central ring peak itself[14]. Planar focusing lenses are more attractive than conventional optical lenses because they are small, lightweight, and easily integrated. A planar plasmonic metalens based on the parabolic phase profile was proposed for the tight focusing of azimuthally polarized light, but the FWHM of the hollow ring was still larger than the diffraction limit[15]. Perfect lenses based on negative refraction have also been proposed for sub-diffraction focusing and imaging with resolution of a few nanometers for visible light[16,17]. However, like those lenses[18–20] utilizing evanescent wave, their working distance is limited within a wavelength. Super-oscillation is an effective way in shaping sub-diffraction optical structure in far-field. To achieve a long working distance, super-oscillatory lenses have been proposed for far-field sub-wavelength focusing beyond the diffraction limit[21–28]. Recently, lenses based on quasi-continuous amplitude modulation[29] and binary amplitude-phase planar mask[30] have been demonstrated for the sub-diffraction focusing of linearly polarized light in experiments. A binary amplitude-phase-mask-based super-oscillation lens was also reported for the sub-diffraction focusing of circularly polarized waves with an ultra-long focal length and small NA[31]. Metamaterials[32,33] are promising building block for super-resolution lens. A lens based on metasurface was reported for ultrabroadband sub-diffraction focusing[34], however present metasurface suffers from

[1]Key Laboratory of Optoelectronic Technology and Systems (Chongqing University), Ministry of Education, and Key Disciplines Lab of Novel Micro-nano Devices and System Technology, Chongqing University, 173 Shazheng Street, Shapingba, Chongqing 400044, China. [2]National Center for Nanoscience and Technology, No. 11 Zhong Guan CunBei Yi Tiao, Beijing 100190, China. [3]State Key Laboratory of Optical Technologies on Nano-Fabrication and Micro-Engineering, Institute of Optics and Electronics, Chinese Academy of Science, P. R. Box 350, Chengdu 610209, China. Correspondence and requests for materials should be addressed to G.C. (email: gchen1@cqu.edu.cn) or Z.-q.W. (email: wenzq@cqu.edu.cn) or L.-r.D. (email: dai@nanoctr.cn)

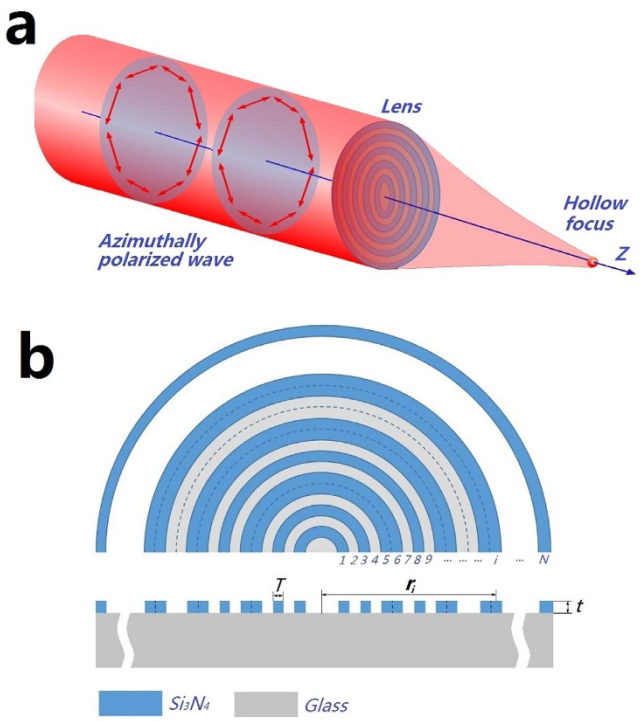

Figure 1. (**a**) Generation of a sub-diffraction hollow ring by shaping the azimuthally polarized wave with a planar binary phase lens, and (**b**) the micro lens structure.

the low transmission rate. Super-oscillartory lenses were also reported for applications, such as super-resolution microscopes[24,35,36] and telescope[37]. This provides a new way to generate a sub-diffraction optical hollow ring. In this paper, we propose a far-field diffractive planar lens based on binary phase mask, which is designed with an ultra-long focal length of 600 λ and a small NA of 0.64. The lens focuses an azimuthally polarized wave into sub-diffraction hollow ring with an FWHM of 0.61 λ, smaller than the diffraction limit 0.78 λ. A small sidelobe level was also observed on the focal plane.

Materials and Methods

Theoretical design of sub-diffraction lens. Figure 1(a) illustrates the generation of the sub-diffraction hollow ring by shaping the azimuthally polarized wave with a planar binary phase lens. The geometrical structure of the lens is depicted in Fig. 1(b). The lens consists of a series of concentric Si_3N_4 rings grown on the top of a glass substrate. The width and the thickness of the rings are T and t, respectively. The binary phase was realized by controlling the Si_3N_4 stripe thickness 0 and t for the phase changes of 0 and π, respectively. The value of t was obtained by $t = \lambda/2(n_{Si3N4}\text{-}1)$, with n_{Si3N4} being the refractive index of Si_3N_4.

A lens based on binary phase modulation was designed for a normally incident wave with an azimuthal polarization at wavelength $\lambda = 632.8$ nm. In the design, the diffracted electrical field was calculated with angular spectrum method[21], and the lens phase spatial distribution was optimized by using particle swarm optimization algorithm[38]. The electrical field of an azimuthally polarized wave can be expressed by the superposition of linearly polarized TEM_{01} and TEM_{10} Gaussian modes[39], as given by Equation 1, where E_0 is the incident electrical field amplitude, w_0 is the beam waist size, $z_0 = \pi w_0^2/\lambda$ is the Rayleigh range, $R(z) = z[1+(z_0/z)^2]$ is the radius of curvature, $w(z) = w_0[1+(z/z_0)^2]^{1/2}$ is the beam width at z, and $k = 2\pi/\lambda$ is the wavenumber.

$$E(r, z) = E_0 \frac{w_0}{w(z)^2} r \exp\left(\frac{-r^2}{w(z)^2}\right) \exp\left\{j\left[kz + \frac{kr^2}{2R(z)} - 2\arctan\left(\frac{z}{z_0}\right)\right]\right\} \quad (1)$$

The incident beam intensity profile is Laguerre–Gaussian with $w_0 = 331$ μm and $z = 276$ mm (Fig. 2(a)), and shows a peak-peak diameter of 830 λ and a hollow ring FWHM of 399.5 λ. According to the vectorial angular spectrum method, there is only an azimuthal component in the electrical field diffracted by the circularly symmetrical lens. The electrical field on the focal plane at $z = z_f$ is given by Equation 2, which was obtained by applied the vectorial angular spectrum diffraction formulas[21,27] to the azimuthally polarized light with circular symmetrical intensity distribution in cylindrical coordinate.

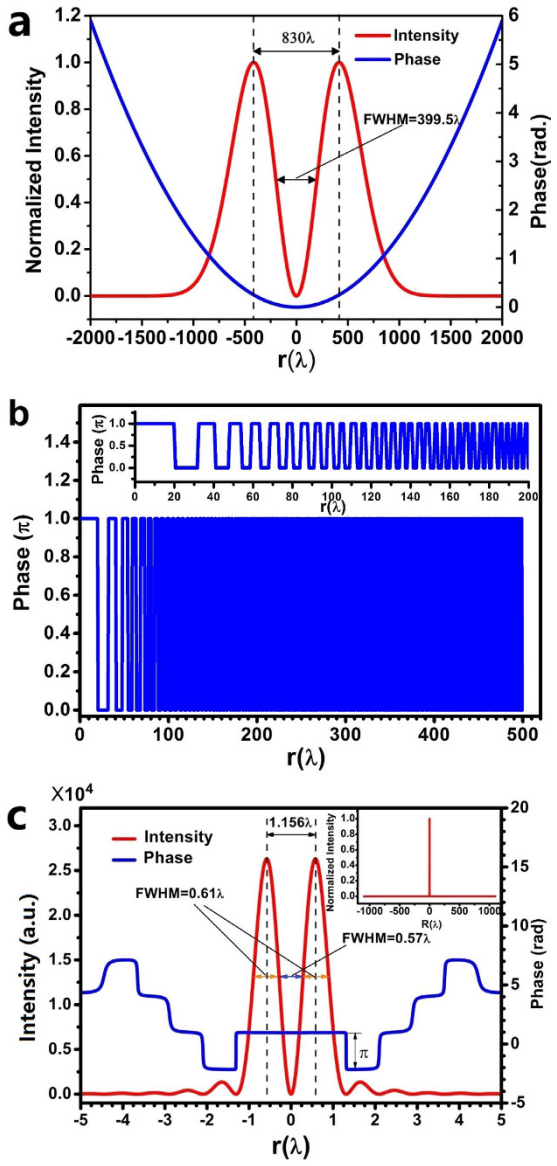

Figure 2. (**a**) The normalized theoretical intensity and phase distribution of the incident azimuthally polarized light; (**b**) the optimized lens phase distribution; (**c**) the designed intensity and phase distribution on the focal plane. The inset of (**b**) is the zoom-in plot of the lens phase distribution and the inset of (**c**) is the normalized intensity on the focal plane.

$$\begin{cases} E_{\varphi}(r, z_f) = \int_0^{\infty} A(\rho)\exp[j2\pi q(\rho)z_f]J_1(2\pi\rho r)2\pi\rho d\rho \\ A(\rho) = \int_0^{\infty} g(r)t(r)J_1(2\pi\rho r)2\pi r dr \end{cases} \quad (2)$$

where φ denotes the polarization direction of the incident light, r and ρ are radial coordinates in the spatial and frequency domains, respectively, $g(r)$ and $t(r)$ are the incident beam electrical field distribution and the lens transmittance function, respectively, J_1 is the first-order Bessel function, and $q(\rho) = (1/\lambda^2\text{-}\rho^2)^{1/2}$.

The radius of the lens is $R = 500\,\lambda$, its focal length is $f = 600\,\lambda$, and its numerical aperture (NA) is $sin[arctan(f/R)] = 0.64$. Therefore, the corresponding diffraction limit is $0.78\,\lambda$ ($0.5\,\lambda$/NA) and the super-oscillation criterion is $0.59\,\lambda$ ($0.38\,\lambda$/NA)[40]. The value of T is 500 nm, which is smaller than the incident wavelength of 632.8 nm. Figure 2(b) gives the optimized phase spatial distribution on the lens in the area with radius less than $120\,\lambda$ (the details of the phase spatial distribution can be found in the supplementary materials, where the phase 0 and π correspond to t_{Si3N4} values of 0 and 348 nm respectively). The theoretically optimized electrical field distribution on the focal plane was depicted with respect to the radial coordinate in Fig. 2(c), which shows the cross-section of the optical hollow ring intensity (red). The peak-peak diameter of the hollow ring is about $1.156\,\lambda$ and the FWHM (as indicated by the blue arrows) is about $0.57\,\lambda$, which is almost half of the

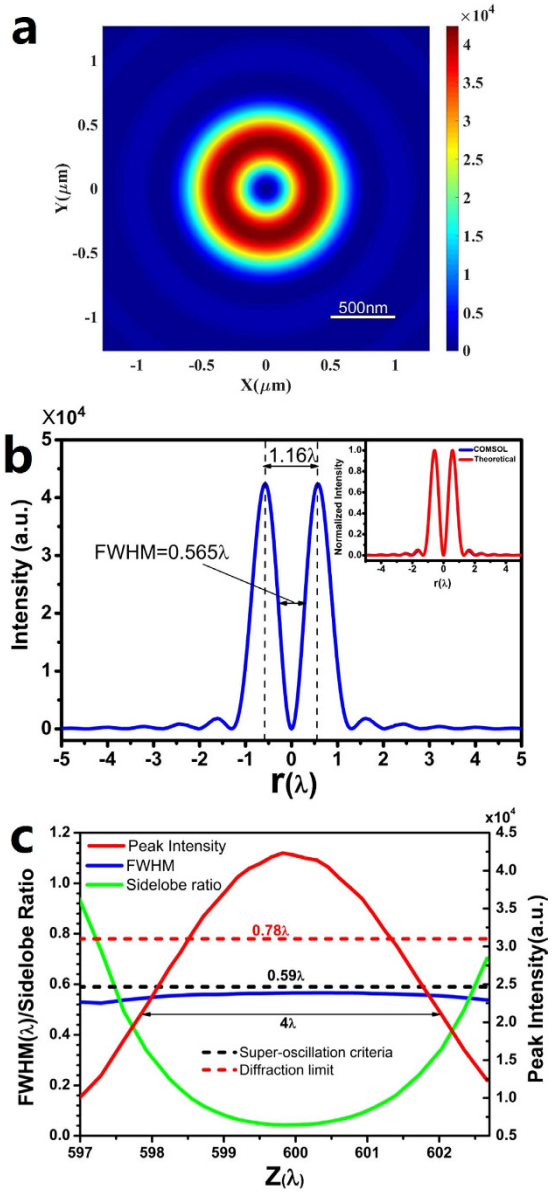

Figure 3. COMSOL Multiphysics simulation results. (**a**) The color map of the intensity distribution on the focal plane; (**b**) the variation of the optical intensity along the radial direction on the focal plane; (**c**) the change in the FWHM, peak intensity, and sidelobe ratio along the propagation axis Z. The inset of (**b**) gives the comparison between the theoretical design and the COMSOL simulation.

peak-peak diameter, and smaller than the diffraction limit of 0.78 λ (0.5 λ/NA) and the super-oscillation criterion of 0.59 λ. The sidelobe intensity on the focal plane was found to be less than 5.1% of the hollow ring peak intensity, leading to a very clear field of view in the region [−1050 λ, +1050 λ], as shown in the inset of Fig. 2(c). We also found that the FWHM of each peak (as indicated by the orange arrows) is about 0.61 λ, which is also smaller than the diffraction limit of 0.78 λ. This sub-diffraction feature was also reflected in the phase distribution (blue curve), which shows a sharp phase inversion, or a phase change of π, at the first minimum at $r = 1.3\,\lambda$. This sharp phase change is a direct evidence of super-oscillation.

Numerical simulations. The COMSOL Multiphysics software was used to conduct the simulation of the optimized lens with real physical Si_3N_4 ring structures. Following the optimized phase distribution, a real lens structure, as given in Fig. 1(b), was constructed in the COMSOL Multiphysics (The detailed structure information can be found in Table 1 in the Supplementary Information). The ring thickness is $t = 348$ nm for phase π and a Si_3N_4 refractive index of 1.91. The parameters of the incident azimuthally polarized wave are the same as those used in the theoretical design. In the simulation, scattering boundary condition and perfectly matched layer was used to avoid unphysical reflection from the boundary. According to the simulation results, the focal length was 599.8 λ, which is quite close to the value of 600 λ in our theoretical design. Figure 3(a) gives the color map

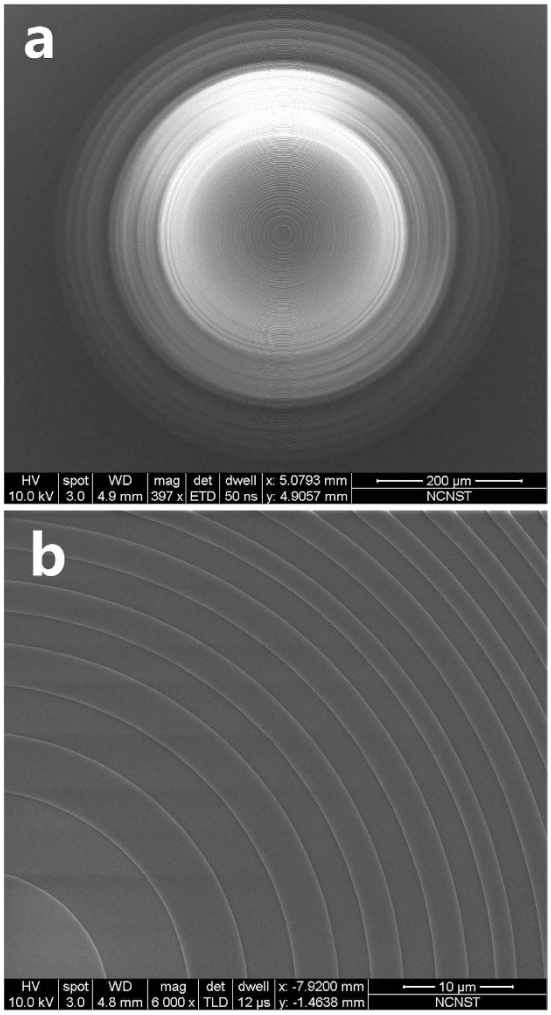

Figure 4. (**a**) The SEM images of the micro lens, and (**b**) the zoom-in of the lens central part.

of the optical intensity on the focal plane. Figure 3(b) plots the corresponding optical intensity against the radial coordinate, which shows a hollow ring FWHM of 0.565 λ and a peak-peak diameter of 1.16 λ. Both the FWHM and the peak-peak diameter are quite close to their corresponding values from the theoretical design. In the inset of Fig. 3(b), the focal plane optical intensity distribution is plotted for both theoretical design and COMSOL simulation for comparison, and two plots show an excellent agreement. According to the COMSOL simulation, the variation of the FWHM, peak intensity, and sidelobe ratio (the ratio of the maximum sidelobe to the peak intensity) were plotted along the optical axis in Fig. 3(c). We found that the FWHM of the hollow ring was smaller than the super-oscillation criterion of 0.59 λ in the area of $597\,\lambda < z < 602.7\,\lambda$ around the focal point $z = 599.8\,\lambda$. In the area of z between 599 λ and 600.8 λ, the sidelobe ratio was less than 10%. The FWHM of the hollow ring in the z direction (propagation direction) was about 4 λ, as indicated by the arrows in Fig. 3(c).

Results and Discussion

Lens fabrication. A micro lens was fabricated using electron-beam lithography and dry etching. The detailed geometrical structure of the micro lens is shown in Table 1 in the Supplementary Information. A 500-μm thick sapphire glass was used as the lens substrate. A Si_3N_4 layer was first deposited on the substrate with PECVD coating, and its refractive index was characterized with ellipsometry, which yielded a refractive index of 1.91. The thickness of this dielectric layer was about 348 nm, corresponding to the relative phase change of π. Dry etching was adopted to form the Si_3N_4 dielectric ring structures. Figure 4(a,b) shows the SEM images of the micro lens.

Experimental setup. To experimentally generate a sub-diffraction optical hollow ring, the incident azimuthally polarized wave was first produced by illuminating an s-wave plate (Workshop of Photonics, Lithuania) with a normal incident linearly polarized Gaussian beam at a wavelength of 632.8 nm from a He-Ne laser. The power of the azimuthally polarized light was about 4 mW. In Fig. 5, the intensity profile of the azimuthally polarized wave on the incident surface was illustrated for five different directions with angles of 0, 0.2 π, 0.4 π, 0.6 π, and 0.8 π crossing the beam's center. The peak-peak diameter and FWHM of the incident azimuthally polarized wave were about 836 λ and 415 λ, respectively, similar to the theoretical values of 830 λ and 399.5 λ, respectively,

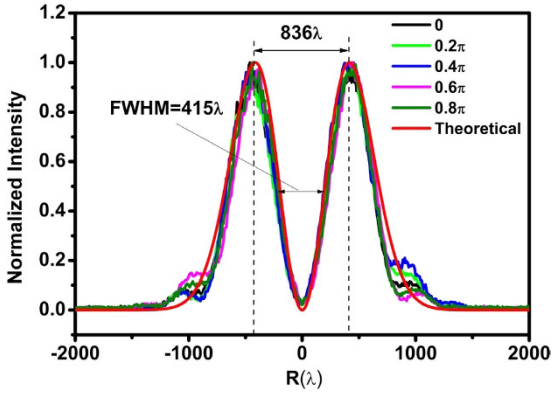

Figure 5. The intensity distribution of the incident azimuthally polarized wave at five different directions with angles of 0, 0.2 π, 0.4 π, 0.6 π, and 0.8 π crossing the beam's center on the lens input surface.

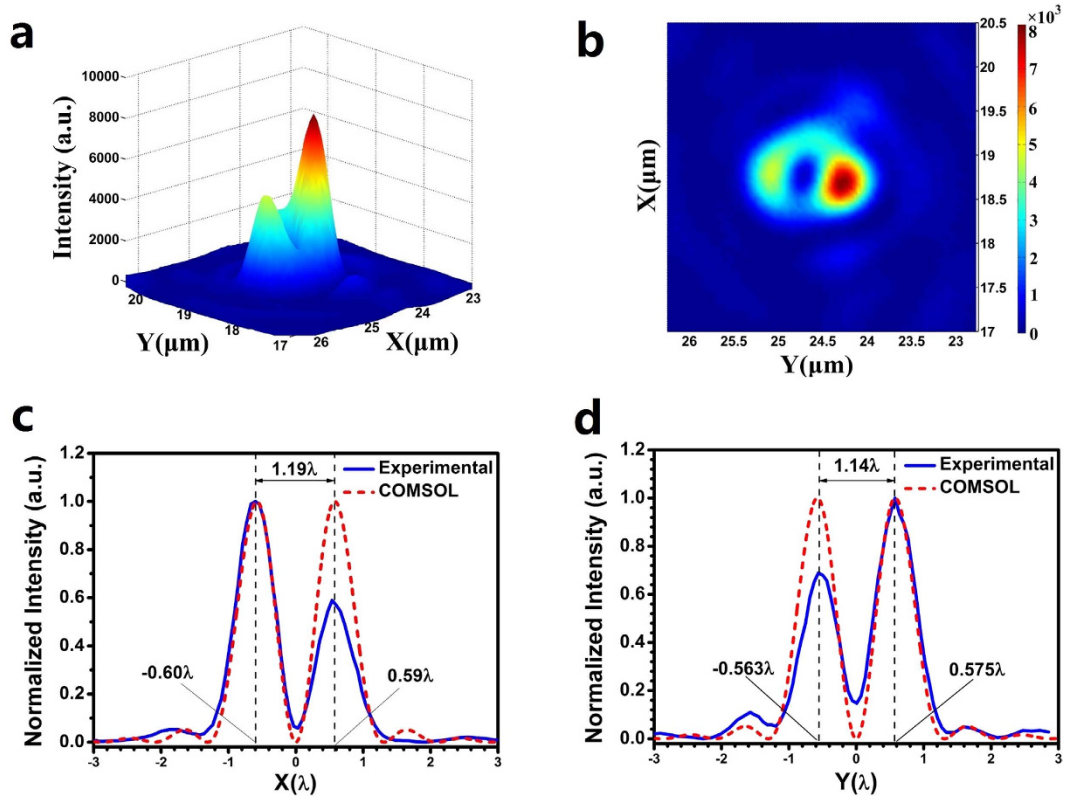

Figure 6. The (**a**) 3D and (**b**) 2D color maps of the measured optical intensity on the focal plane; the optical intensity distribution along the (**c**) x-axis and (**b**) y-axis.

in the design (Fig. 2(a)). We also noticed that the intensity distribution did not exhibit perfectly circular symmetry because of difficulties in optical alignment.

In the experiment, the azimuthally polarized wave was normally incident on the lens from the substrate side. The diffracted optical intensity distribution was measured after the lens with a tapered optical fiber probe (CFN-100 of Nanonics Imaging, Ltd., Israel) mounted on a 3-D piezo nanopositioner (P-561.3CD of Physik Instrumente GmbH & Co., Germany). The probe tip diameter was 100 nm. Although the probe size has convolution effect on the experimental result, it was found to be small and can be ignored in our case. The spatial resolution and scanning range of the nanopositioner were about 10 nm and 100 μm, respectively, for each of the x, y, and z axes. The collected photons were detected by a single photon detector (SPCM50A/M of Thorlabs, Inc., USA). By moving the 3-D nanopositioner, the fiber probe was able to scan the optical intensity distribution in the plane perpendicular to the optical axis at different distances.

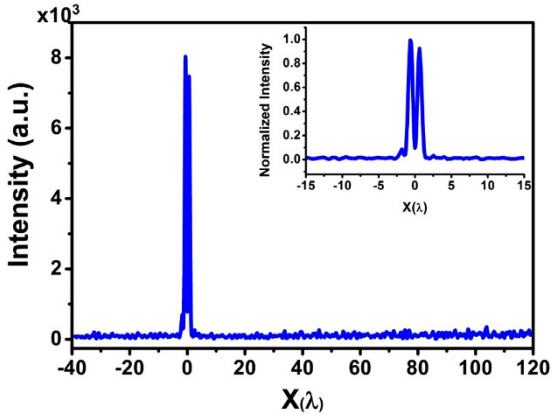

Figure 7. The optical intensity distribution taken in a large range in the x-direction across the focus center on the focal plane.

Experimental generation of sub-diffraction hollow ring. The focal plane was found to be approximately 380 μm (600.5 λ), which was similar to the theoretically predicted value of 600 λ and the COMSOL simulation result of 599.8 λ. Figure 6(a,b) give the 3D and 2D color maps of the optical intensity measured on the focal plane, which show a clear hollow ring structure. Due to the difficulties in the optical alignment mentioned above, the focal hollow ring was not symmetrical. The optical intensity varied around the circumference of the central peak lobe. To evaluate the size of the hollow ring, the normalized intensity distribution was plotted along the x direction and y direction across the center of the hollow ring in Fig. 6(c,d), respectively. The peak-peak diameter of the hollow ring was 1.19 λ and 1.14 λ in the x direction and y direction, respectively, and these values are quite close to the value of 1.16 λ obtained in the COMSOL simulation, depicted in Fig. 3(b). For further comparison, the normalized COMSOL simulation result is also given in the Fig. 6(c,d).

Except for the symmetry, the experimental results show a good agreement with the intensity shape from the theoretical simulation. The hollow ring FWHM is 444 nm (0.702 λ) and 356 nm (0.563 λ) in the x direction and y direction, respectively, and both are smaller than the diffraction limit of 0.78 λ. The FWHM in the y direction is even smaller than the super-oscillation criterion of 0.59 λ. To better evaluate the hollow ring's size, the FWHM was measured along the 16 different directions with equal angle steps of 24°. We obtained an average FWHM of 386 nm (0.61 λ), which was smaller than the diffraction limit of 0.78 λ and close to the super-oscillation criterion of 0.59 λ. The corresponding average peak-peak diameter was about 720 nm (1.14 λ), which is also similar to the COMSOL simulation result of 1.16 λ, as shown in Fig. 3(b). A long-range scan was taken along the x direction to investigate a large area of optical intensity on the focal plane, as shown in Fig. 7, which gives a clear field of view in the area of [−39 λ, 120 λ]. The measured maximum sidelobe was less than 10% of the maximum peak intensity. Numerical investigation was conducted to find out the influence of fabrication error and optical misalignment on the optical intensity distribution on the focal plane. It was found that off-axis incident and tilted incident have major contributions to the asymmetrical optical intensity distribution on the focal plane.

Conclusions

It has been demonstrated that a sub-diffraction hollow ring structure can be obtained in the far-field by shaping an azimuthally polarized wave with a micro planar lens based on the binary phase mask. The planar lens was designed and fabricated with an ultra-long focal length of 600 λ and small NA of 0.64. Experimental results showed that a hollow ring was generated with an FWHM of 0.61 λ, which is smaller than the diffraction limit of 0.78 λ. The measured peak-peak diameter of the hollow ring was about 1.14 λ and the sidelobe's ring intensity was less than 10% of the central lobe's maximum intensity. Compared with conventional lenses, sub-diffraction lenses can achieve the same FWHM with smaller NA, and therefore realize a much longer focal length and working distance, which is important for detecting the information deep inside the sample. A hollow ring with FWHM smaller than 0.36 λ (or even smaller) is also expected to be achieved by further increasing the NA value and employing more phase values during the design and fabrication stages. Such a sub-diffraction planar lens with an ultra-long focal length has great potential in further improving the optical resolution of stimulated emission depletion (STED) microscopy, optical tweezers, and nanolithography. This planar lens is also attractive due to its unique properties, including its small size, light weight, and ability to be easily integrated. This method can also be adopted for the generation of sub-diffraction hollow ring in other spectrum ranges, such as infrared and terahertz.

References

1. Zhan, Q. Cylindrical vector beams: from mathematical concepts to applications. *Adv. Opt. Photon.* **1,** 1–57 (2009).
2. Hell, S. W. Far-field optical nanoscopy. *Science* **316,** 1153–1158 (2007).
3. Zhang, D. W. & Yuan, X. C. Optical doughnut for optical tweezers. *Opt. Lett.* **28,** 740–742 (2003).
4. Gan, Z., Cao, Y., Evans, R. A. & Gu, M. Three-dimensional deep sub-diffraction optical beam lithography with 9 nm feature size. *Nat. Comm.* **4,** 1–7 (2013).

5. Kuang, C., Liu, Y., Hao, X., Luo, D. & Liu, X. Creating attoliter detection volume by microsphere photonic nanojet and fluorescence depletion. *Opt. Commun*. **285,** 402–406 (2012).
6. Hao, X. A., Kuang, C. F., Wang, T. T. & Liu, X. Phase encoding for sharper focus of the azimuthally polarized beam. *Opt. Lett*. **35,** 3928–3930 (2010).
7. Youngworth, K. & Brown, T. Focusing of high numerical aperture cylindrical-vector beams. *Opt. Exp*. **7,** 77–87 (2000).
8. Helseth, L. E. Smallest focal hole. *Opt. Commun.* **257,** 1–8 (2006).
9. Zhan, Q. & Leger, J. Focus shaping using cylindrical vector beams. *Opt. Exp*. **10,** 324–331 (2002).
10. Yuan, G. H., Wei, S. B. & Yuan, X. C. Nondiffracting transversally polarized beam. *Opt. Lett*. **36,** 3479–3481 (2011).
11. Tian, B. & Pu, J. Tight focusing of a double-ring-shaped, azimuthally polarized beam. *Opt. Lett*. **36,** 2014–2016 (2011).
12. Lalithambigai, K. *et al.* Generation of subwavelength super-long dark channel using high NA lens axicon. *Opt. Lett*. **37,** 999–1001 (2012).
13. Hao, X., Kuang, C., Wang, T. & Liu, X. Manipulation of doughnut focal spot by image inverting interferometry. *Opt. Lett*. **37,** 821–823 (2012).
14. Chen, W. *et al.* Large scale manipulation of the dark spot by phase modulation of azimuthally polarized light. *Opt. Commun*. **349,** 125–131 (2015).
15. Luo, J. *et al.* Tight focusing of radially and azimuthally polarized light with plasmonic metalens. *Opt. Commun*. **356,** 445–450 (2015).
16. Pendry, J. B. Negative refraction makes a perfect lens. *Phys. Rev. Lett.* **85,** 3966 (2000).
17. Fang, N., Lee, H., Sun, C. & Zhang, X. Sub-diffraction-limited optical imaging with a silver superlens. *Science* **308,** 534–537 (2005).
18. Luo, J. *et al.* Fabrication of anisotropically arrayed nano-slots metasurfaces using reflective plasmonic lithography. *Nano Scale* **7,** 18805 (2015).
19. Gao, P. *et al.* Enhancing aspect profile of half-pitch 32 nm and 22 nm lithography with plasmonic cavity lens. *Appl. Phys. Lett.* **106,** 093110 (2015).
20. Zhao, Z. *et al.* Going far beyond the near-field diffraction limit via plasmonic cavity lens with high spatial frequency spectrum off-axis illumination. *Sci. Rep*. **5,** 15320 (2015).
21. Kotlyar, V. V. *et al.* Analysis of the shape of a subwavelength focal spot for the linearly polarized light. *Appl. Opt*. **52,** 330–339 (2013).
22. Yuan, G. *et al.* Planar super-oscillatory lens for sub-diffraction optical needles at violet wavelengths. *Sci. Rep*. **4,** 6333 (2014).
23. Rogers, E. T. F. *et al.* A super-oscillatory lens optical microscope for subwavelength imaging. *Nat. Mater*. **11,** 432 (2012).
24. Rogers, E. T. F. & Zheludev, N. I. Optical super-oscillations: sub-wavelength light focusing and super-resolution imaging. *J. Opt.* **15,** 094008 (2013).
25. Yuan, G., Rogers, E. T. F., Roy, T., Shen, Z. & Zheludev, N. I. Flat super-oscillatory lens for heat-assisted magnetic recording with sub-50 nm resolution. *Opt. Exp*. **22,** 6428–6437 (2014).
26. Qin, F. *et al.* Shaping a subwavelength needle with ultra-long focal length by focusing azimuthally polarized light. *Sci. Rep*. **5,** 09977 (2015).
27. Liu, T., Tan, J. B., Liu, J. & Wang, H. T. Vectorial design of super-oscillatory lens. *Opt. Exp*. **21,** 15090–15101 (2013).
28. Wen, Z. Q., He, Y. H., Li, Y. Y., Chen, L. & Chen, G. Super-oscillation focusing lens based on continuous amplitude and binary phase modulation. *Opt. Exp*. **22,** 22163–22171 (2014).
29. Chen, G. *et al.* Super-oscillation far-field focusing lens based on ultra-thin width-varied metallic slit array. *IEEE Photon. Technol. Lett*. **28,** 335–338 (2016).
30. Chen, G. *et al.* Far-field sub-diffraction focusing lens based on binary amplitude-phase mask for linearlypolarized light. *Opt. Exp*. **24,** 11002–11008 (2016).
31. Chen, G. *et al.* Super-oscillatory focusing of circularly polarized light by ultra-long focal Length planar lens based on binary amplitude-phase modulation, *Sci. Rep*. **6,** 29068 (2016).
32. Smith, D. R., Pendry, J. B. & Wiltshire, M. C. K. Metamaterials and negative refractive index. *Science* **305,** 788–792 (2004).
33. Shen, Y., Ko, H. Y., Ai, Q., Peng, S. M. & Jin, B. Y. Molecular split-ring resonators based on metal string complexes. *J. Phys. Chem. C* **118,** 3766 (2014).
34. Tang, D. *et al.* Ultrabroadband superoscillatory lens composed by plasmonic metasurfaces for subdiffraction light. *Laser and Photonics Reviews* **9,** 713–719 (2015).
35. Huang, F. M. & Zheludev, N. I. Super-resolution without evanescent waves. *Nano Lett.* **9,** 1249–1254 (2009).
36. Wong, A. M. H. & Eleftheriades, G. V. An optical super-microscope for far-field, real-time imaging beyond the diffraction limit. *Sci. Rep.* **3,** 1715 (2013).
37. Wang, C. *et al.* Super-resolution optical telescopes with local light diffraction shrinkage. *Sci. Rep*. **5,** 18485 (2015).
38. Jin, N. & Rahmat-Samii, Y. Advances in particle swarm optimization for antenna designs: real-number, binary, single-objective and multi-objective implementations. *IEEE Trans. Antenn. Propag.* **55,** 556–567 (2007).
39. Nesterov, A. V. & Niziev, V. G. Laser beams with axially symmetric polarization. *J. Phys. D Appl. Phys.* **33,** 15 (2000).
40. Huang, K. *et al.* Optimization-free superoscillatory lens using phase and amplitude masks. *Laser Photon. Rev*. **8,** 152–157 (2014).

Acknowledgements

The authors would like to acknowledge the financial support from the China National Key Basic Research and Development Program under Grant No. 2013CBA01700. This work was also supported by the China National Natural Science Foundation under Grant Nos 61575031 and 61177093, the Program for New Century Excellent Talent in University (NCET-13-0629), the Scientific Research Foundation for the Returned Overseas Chinese Scholars, State Education Ministry, the Fundamental Research Funds for the Central Universities (projects 106112013CDJZR120019, 106112016CDJZR125503 and 106112015CDJXY120012), and Chongqing advanced and applied basic research project(cstc2015jcyjA40020). Authors also thank LetPub (www.letpub.com) for their linguistic assistance during the preparation of this manuscript.

Author Contributions

G.C. conceived the idea and carried out the lens design. Z.X.W. performed the numerical simulations. K.Z. fabricated the lens samples. S.L.J., L.C. and L.R.D. helped in fabricating lens samples. G.C., Z.Z.Z., L.R.D. and Z.Q.W. designed and built up the experimental system. Z.X.W., A.P.Y. and Y.Y.L. conducted the experiment. Z.X.W. and G.C. analyzed the data. C.T.W. and X.G.L. gave helpful suggestions in the design. G.C. prepared the manuscript.

Additional Information

Supplementary information accompanies this paper at http://www.nature.com/srep

Competing financial interests: The authors declare no competing financial interests.

How to cite this article: Chen, G. *et al.* Generation of a sub-diffraction hollow ring by shaping an azimuthally polarized wave. *Sci. Rep.* **6**, 37776; doi: 10.1038/srep37776 (2016).

Publisher's note: Springer Nature remains neutral with regard to jurisdictional claims in published maps and institutional affiliations.

This work is licensed under a Creative Commons Attribution 4.0 International License. The images or other third party material in this article are included in the article's Creative Commons license, unless indicated otherwise in the credit line; if the material is not included under the Creative Commons license, users will need to obtain permission from the license holder to reproduce the material. To view a copy of this license, visit http://creativecommons.org/licenses/by/4.0/

© The Author(s) 2016